International Journal of Rock Mechanics & Mining Sciences 137 (2021) 104555

Contents lists available at ScienceDirect

International Journal of Rock Mechanics and Mining Sciences

journal homepage: http://www.elsevier.com/locate/ijrmms

Feasibility of constructing a full-scale radioactive high-level waste disposal cell and characterization of its thermo-hydro-mechanical behavior

Frédéric Bumbieler [a,*], Carlos Plúa [b], Saeed Tourchi [c], Minh-Ngoc Vu [a], Jean Vaunat [c], Antonio Gens [c], Gilles Armand [b]

[a] Andra, Châtenay-Malabry, France
[b] Andra, Meuse/Haute Marne Underground Research Laboratory, Bure, France
[c] Universitat Politècnica de Catalunya, Department of Civil and Environmental Engineering, Barcelona, Spain

ARTICLE INFO

Keywords:
In-situ experiments
THM behavior
Thermal pressurization
Claystone
Buried steel sleeve
Numerical simulation

ABSTRACT

Within the context of deep geological radioactive waste disposal, the French National Radioactive Waste Management Agency (Andra) is conducting a research program including in-situ experiments at the Meuse/Haute-Marne Underground Research Laboratory (MHM URL), which aims to demonstrate the feasibility of constructing and operating a High Level Waste (HLW) disposal facility in the Callovo-Oxfordian (COx) claystone formation and to improve it. ALC1604 experiment is an in-situ heating test reproducing a full-scale HLW disposal cell. Heating devices were placed in the last 15 m of a 25 m long steel cased micro-tunnel to mimic the heat emitted by the HLW packages. The present experiment allows to study the response of the cell and the surrounding rock under thermal loading. More specifically, this experiment studied the thermo-mechanical (TM) behavior of the steel sleeve, equipped with strain gauges, displacement sensors, temperature sensors, etc., and monitored the evolution of the annular space (the gap between the sleeve and the rock). It also studied the thermo-hydro-mechanical (THM) behavior of the near/far field rock through pore pressure and temperature measurements installed in peripheral boreholes. The TM response of the steel sleeve and the THM response of the surrounding rock are numerically reproduced and the chosen THM parameters are compared with previous small-scale in-situ experiments conducted at the MHM URL in order to improve the reliability of the material parameters of the COx. The lessons learned from this experiment has provided valuable feedback towards implementing new full-scale heating experiments consistent with a new benchmark concept.

1. Introduction

The French National Radioactive Waste Management Agency (Andra), is in charge of studying the disposal of high-level and intermediate-level long-lived waste (HLW and ILW-LL) in a deep geological repository (Cigéo project) which will be located at the border of the Meuse and Haute-Marne departments, nearly 300 km East of Paris. The host formation consists of a claystone (Callovo-Oxfordian argillaceous rock – COx) lying between 420 m and 550 m in depth and exhibiting very favorable conditions for a repository of radioactive waste, as they generally have a very low hydraulic conductivity, small molecular diffusion and significant retention capacity for radionuclide. The underground disposal facility will be divided into two sections depending on the type of waste (ILW-LL or HLW) and the type of excavation used to emplace the waste disposal packages (tunnel of 9–11 m in diameter for ILW-LL and steel cased micro-tunnel of about 0.7 m in inner diameter for HLW).

Heat released from the most exothermic HLW packages leads to temperature increase of the sleeve up to 90 °C after a few years. Thermal loading leads to pore pressure increase due to the difference in thermal expansion coefficients between pore water and solid skeleton of COx claystone.[1–5] It also leads to an increase of radial loading applied on the sleeve due to thermal expansion of the rock. If the mechanical behavior of buried steel pipelines is widely studied by oil and gas industry,[6] for these applications, large displacement but small confinement pressure are usually considered to design the pipeline and verify its structural integrity (leak tightness retention) under seismic loadings and landslides. Within the framework of the feasibility study of geological repositories for HLW, the structural performance of deep buried steel sleeve subjected to high confinement pressure and small displacement

* Corresponding author.
E-mail address: frederic.bumbieler@andra.fr (F. Bumbieler).

https://doi.org/10.1016/j.ijrmms.2020.104555
Received 6 April 2020; Received in revised form 16 October 2020; Accepted 20 November 2020
Available online 15 December 2020
1365-1609/

has to be determined. Thermo-hydro-mechanical (THM) behavior of surrounding rock and resulting overloads applied on the sleeve are therefore key parameters for design and safety assessments.

This paper presents the design, main objectives and results of a full-scale in-situ heating experiment performed at the Meuse/Haute-Marne Underground Research Laboratory (MHM URL) located at some 490 m deep in the middle of the COx claystone layer. After a brief review of the industrial context, the third section describes the experimental device. The results are presented and discussed in the fourth section. Finally some numerical simulations of THM behavior of the rock and thermo-mechanical (TM) behavior of the sleeve are presented in the fifth section.

2. Industrial context and objectives of the experiment

2.1. HLW disposal cell concept

HLW is mainly issued from nuclear plant spent fuel reprocessing activities. They are inserted into a vitrified matrix, and hot cast into stainless steel canisters (thus forming what is called "primary packages") which will be conditioned in thick steel overpacks to prevent glass leaching until the glass matrix temperature has decreased below 50/70 °C depending on the type of waste. The main function of this overpack is thus to prevent water from reaching the glass matrix during 500 years for the most exothermic waste. P285NH non-alloy ductile steel has been chosen to fulfill this requirement.[7]

These overpacks will be stored in disposal cells that are sub-horizontal dead-end micro-tunnels with an excavated diameter of approximately 0.9 m, oriented according to the direction of major stress σ_H in the COx formation. The disposal cell comprises a head part for the cell closure and a useable disposal part containing the disposal packages and spacers if applicable (to control the thermal output of a disposal cell, Fig. 1). Based on the reference design adopted at the end of the basic engineering design stage, the length of the cell is of the order of 150 m for the exothermic HLW and of the order of 80 m for the moderately exothermic HLW which will be emplaced in a few cells during a pilot phase. To prevent rock deformation and enable potential retrieval of disposal packages during the reversibility period (i.e., about 100 years), the cell is equipped with a non-alloy steel sleeve. The final design of the HLW cells is not fixed yet and technological optimizations are still in progress. Ongoing research and development has for instance led in 2015 to (i) choose an oil-grade ferritic-pearlitic steel for the sleeve (API 5L X65 MS) to improve its stress corrosion cracking resistance[8] and (ii) fill the annular gap between the sleeve and the clay rock with a material that imposes corrosion-limiting environmental conditions (cement-based grout).

2.2. Contribution of MHM URL to HLW disposal cell design and THM behavior

In 2000, Andra began to build the so-called Meuse/Haute-Marne Underground Research Laboratory (MHM URL) in order to conduct experiments to establish the feasibility of constructing and operating a radioactive waste disposal facility in the COx claystone. The URL is located at some 490 m deep in the middle of the COx claystone layer. In-situ stress field is anisotropic at the level of the URL. The major stress (σ_H) is horizontally oriented at NE155° equals to −16 MPa. Vertical stress (σ_v) and horizontal minor stresses (σ_h) are about −12 MPa. This anisotropic stress state which is consistent with the one given for the east of the Paris basin relative to the thrust of the Alps, has been confirmed by an important characterization of in-situ stress field carried out on a regional scale.[9]

The COx at the MHM URL shows a slight anisotropy for most rock properties; particularly in terms of solute diffusion, water permeability, thermal diffusivity and mechanical parameters. This is due to the alignment of carbonate and tectosilicate inclusions parallel to the bedding plane observed on mineral distribution maps.[10]

Table 1 summarizes the main thermo-hydro-mechanical parameters determined from laboratory tests and in-situ measurements. At the main level of the URL, porosity is approximately 18% with very small mean pore diameter (about 0.02 μm) leading to a very low permeability (ranging between 5.0×10^{-21} m^2 and 5.0×10^{-20} m^2) and a slight anisotropy ratio of about 3. The specific heat capacity of the solid phase is equal to 800–820 J/kg/K, resulting in a specific heat capacity for the whole saturated material of about 1000 J/kg/K.[2] The values for the thermal conductivity of the COx are about 1.9 and 1.3 W/m/K parallel and perpendicular to the bedding plane, respectively. The Young's modulus perpendicular to bedding is around 4.0×10^9 Pa with anisotropy ratio of 1.3, although this ratio can reach 2 for some samples tested on triaxial tests.[11] A detailed summary of the THM behavior of the COx can be found in Ref. 12.

After a first research phase (2000–2005) dedicated to characterization of the confining properties of the clay,[13] a new experimental program focusing more on technical feasibility of the different disposal facilities and on characterization of the rock behavior under representative THM loadings was launched. Full-scale in-situ experiments started in 2009, first to verify that it is possible to drill micro-tunnels in several

Table 1
Callovo-Oxfordian claystone parameters.

Parameter	Unit	Value
Porosity[12]	–	~0.18
Intrinsic permeability[11]	m^2	5.0×10^{-20} - 5.0×10^{-21}
Equivalent heat capacity[2]	J/kg/K	1000
Thermal conductivity parallel to bedding[12]	W/m/K	~1.9
Thermal conductivity perpendicular to bedding[12]	W/m/K	~1.3
Equivalent density[11]	kg/m^3	2400
Volumetric coefficient of thermal expansion[1]	1/K	4.2×10^{-5}
Young's Modulus perpendicular to bedding[11]	Pa	~4.0×10^9

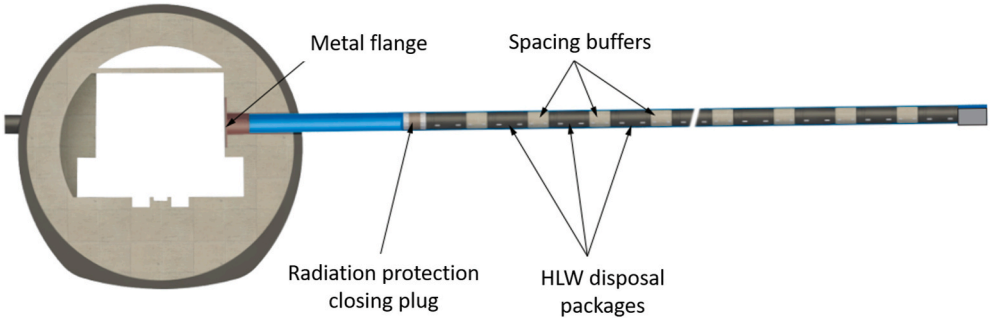

Fig. 1. Exothermic HLW disposal cell.

directions with respect to the in-situ stress field and to emplace a steel sleeve.[14] Excavation of dead-end micro-tunnels required a specific laser guided micro TBM allowing the sleeve emplacement at the same time of the drilling with a maximum initial annular space between the sleeve and the rock of 25 mm.

The mechanical loading process of the sleeve of a cell parallel to σ_H is described in Ref. 15, based on different in-situ experiments at different scales. An anisotropic loading resulting from the anisotropy of the excavation-induced fracture network around the cell is systematically observed. It results in the radial bending of the sleeve and the amplitude of its ovalization will depend on (i) the ratio of convergence rate between horizontal and vertical directions, (ii) the bending stiffness of the sleeve and (iii) the size of the initial gap between the sleeve and the cell wall. Sleeve convergence (and divergence) rates decrease with time and become lower than 10^{-11} s^{-1} after a few years. A progressive decrease in load anisotropy can also be observed.

Several reduced scale heating experiments (so-called TER, TED and TEC experiments) have already been performed at the MHM URL[12] to characterize the THM coupling, analyze sensitivity to the COx parameters and estimate the influence of a thermal loading on mechanical behavior of a 1:5 scale steel sleeve. The results obtained led to (i) a better understanding of far field pore pressure increase under thermal loading which can be reproduced by thermo-poro-elasticity, (ii) the confirmation of elastic moduli, thermal conductivity and permeability anisotropy of COx claystone and (iii) the highlighting of sleeve circumferential mechanical strain increase with temperature for moderate thermal loading.

2.3. Objectives of the experiment ALC1604

The so-called ALC1604 experiment has been implemented at the MHM URL to characterize the behavior of a full-scale HLW cell under a power monitored thermal loading (as it will be the case when waste packages will be stored in the disposal cell). The first objective is to study the influence of heat loading on the mechanical behavior of a buried steel sleeve including the occurrence of overloads resulting from rock mass thermal expansion. This experiment will also provide additional data concerning THM behavior of COx claystone mainly in terms of pore pressure increase induced by the heating phase. The goal here is (i) to confirm THM behavior identified on small-scale heating experiments and (ii) to validate and improve THM modelling.

3. Experimental set-up

3.1. Cell characteristics and heating device

ALC1604 disposal cell was drilled in 2012 and is therefore representative of the initial concept (i.e. without backfilling of annular space between the sleeve and the rock). The cell is 25 m long and is divided into two parts (Fig. 2a): a head part of 6 m long with an excavated diameter of 0.791 m and a useable part of 19 m long with an excavated diameter of 0.75 m. The head part is equipped with an insert 0.767 m in outer diameter and 21 mm thick, and the useable part with a sleeve 0.70 m in outer diameter and 20 mm thick. Both sleeve and insert are made of S235 structural steel having a yield strength of 235 MPa. There is an overlap zone 1 m width between the sleeve and the insert. The difference in diameter between useable part and head makes it possible to accommodate longitudinal thermal expansion of the useable part sleeve and thus avoid additional radial loads on the drift wall.

Before the installation of the instrumentation, a 3D scan showed that the cell trajectory was close to the theoretical one, with a maximum deviation of 3 cm in the horizontal plane and 8 cm in the vertical plane.

The heating is applied in the useable part between 10 and 25 m from the drift wall (Fig. 2a); the heating device is made up of five stainless steel heater elements (H1 to H5) almost centered in the cell. Each heater element is 3 m long, has a diameter of 0.508 m, and contains two electrical resistors controlled through a power regulation system. Once the heating device was emplaced in the cell, two unsealed steel plates were installed: one at the sleeve/insert transition and one at the head of insert in the GAN drift.

Apart from the length of the cell (25 m instead of 80 or 150 m), the rest of characteristics met the requirements for proving the initial reference design of HLW disposal cells. According to the performed numerical simulations for its design, a 25 m long cell including a 15 m long heated zone, was considered sufficiently representative to provide an understanding of the behavior of both the cell and the surrounding rock and more adequate from experimental/technological point of view to perform a heating test, knowing that excavation of real length cells has been fulfilled in other experiments.[15]

3.2. Sleeve and insert instrumentation

The sleeve and insert are made of thirteen 2 m long steel elements, 10 in the useable part and 3 in the head part. Six elements have been

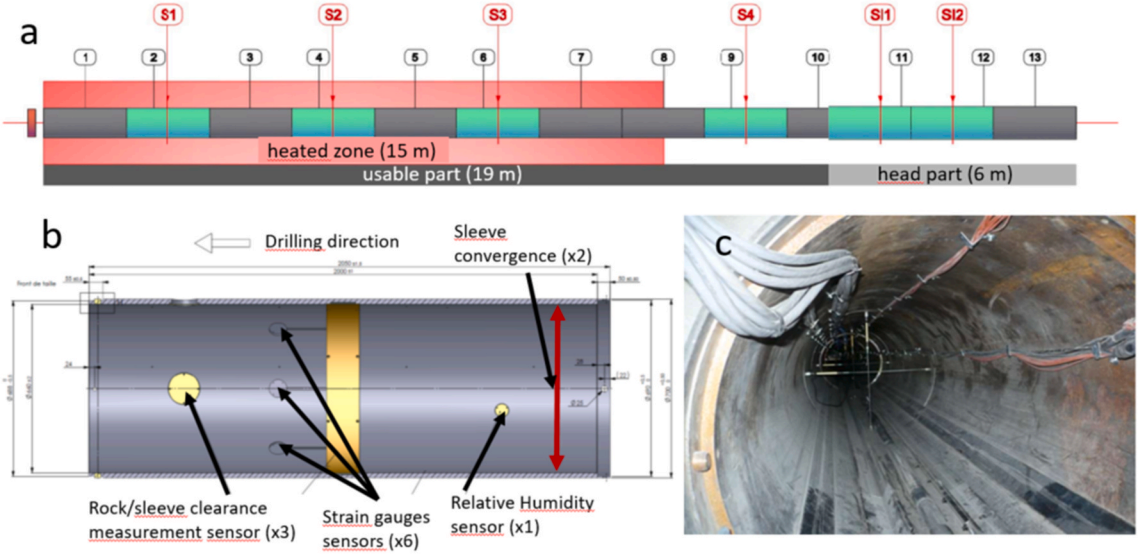

Fig. 2. a) Schematic view of the sleeve and insert elements (Sections S1 to S4 and SI1 to SI2 refer to location of instrumentation of sleeve and insert respectively) – b) Location of the different sensors installed on sleeve/insert elements – c) Convergence sensors in the cell.

instrumented to characterize their TM behavior (sections S1 to S4 for the sleeve and SI1 and SI2 for the insert, Fig. 2a). Each instrumented element was equipped with six strain gauges sectors on the sleeve/insert intrados, with an axial and a circumferential gauge for each sector; these sectors are positioned horizontally and at ± 45° from horizontal direction (Fig. 2b). The gauges are thermally-compensated so that measurements give directly the mechanical strain. Relative humidity/temperature sensors taking a measurement in the annular space 15° below the horizontal axis for each sleeve instrumented element and in the cell for each insert instrumented element, have also been installed.

In addition, sleeve elements 2, 4, 6 and 9 were equipped with three rock/sleeve clearance measuring sensors, one at each side and one in the vault. Sleeve element 9 and insert elements 11 and 12 were equipped with two potentiometric displacement sensors for measuring horizontal and vertical diameter variation (Fig. 2c). Three potentiometric displacement sensors fixed to the insert intrados and resting on the useable part's head plate measure the relative displacement of the sleeve in the insert. Lastly, two PT100 temperature sensors 15° from the vertical axis and 15° above the horizontal axis measure the temperature of each element.

3.3. Peripheral instrumentation

To study the THM behavior of the surrounding rock, nine peripheral boreholes were drilled from the GAN drift and the GRD drift (parallel to the cell axis, Fig. 3). Six boreholes were equipped with pore pressure piezometer chambers associated with temperature sensors: two monopacker boreholes (ALC4001 and ALC4002, the latter appeared to be defective), two multipacker boreholes with five chambers (ALC4005 and ALC1616), and two multipackers boreholes with three chambers (ALC1617 and ALC1618). These boreholes were backfilled with resin in order to ensure sealing and with low compressibility. Two boreholes were equipped with five temperature sensors (ALC4003 and ALC1633). One borehole (ALC4004) was equipped with a magnet extensometer (Mag-X) measuring displacement at 20 different positions along the axis of the borehole. Due to some uncertainties about the validity of these measurements, they are not presented in this paper.

Most of the peripheral boreholes (ALC4001 to ALC4005, ALC1616 and ALC1617) were drilled and equipped about 1 year before the ALC1604 cell excavation to characterize hydro-mechanical impact of the drilling of the cell. Temperature measurement boreholes ALC4003 and ALC1633 were drilled after the ALC1604 cell excavation.

The access drift instrumentation (OHZ1605 to 1608, OHZ1685 to 1688), in the immediate vicinity of the cell head, consisted of temperature sensors, support instrumentation (strain gauges and displacement sensors on sliding steel arches), displacement and tilt sensors to measure drift wall deformation induced by thermal gradient along the cell.

4. Experimental results and interpretation

4.1. Heating phase

To validate the operation of the heaters regulation system and the measurements acquisition, a heating test at low power (33 W/m) was first conducted lasting 2 weeks. The main heating phase started one month later, at a constant nominal power of 220 W/m for the 15 m occupied by the heater elements. This value was designed to reach a temperature of 90 °C at the sleeve after two years. After almost 6 years, heating was stopped in successive cooling stages.

A few breakdowns caused by the control cabinet fans failing occurred during the experiment on one single heater element at a time. These breakdowns did not disrupt the global temperature in the sleeve given that the other four heater elements continued to work well as it will be explained in the next section.

4.2. Surrounding rock

4.2.1. Temperature

Fig. 4 shows the temperature evolution measured by the sensors installed in the peripheral boreholes ALC1616 and ALC1617. These two boreholes are located in the horizontal and vertical plane of the cell, respectively, but only ALC1616_03 and ALC1617_03 were located at the same distance from the wall. Unfortunately, ALC1617_03 was damaged from the beginning of the experiment and no data were recorded. Therefore, it was not possible to study the anisotropic thermal properties of the COx as it was done in Ref. 3. Nevertheless, these measurements

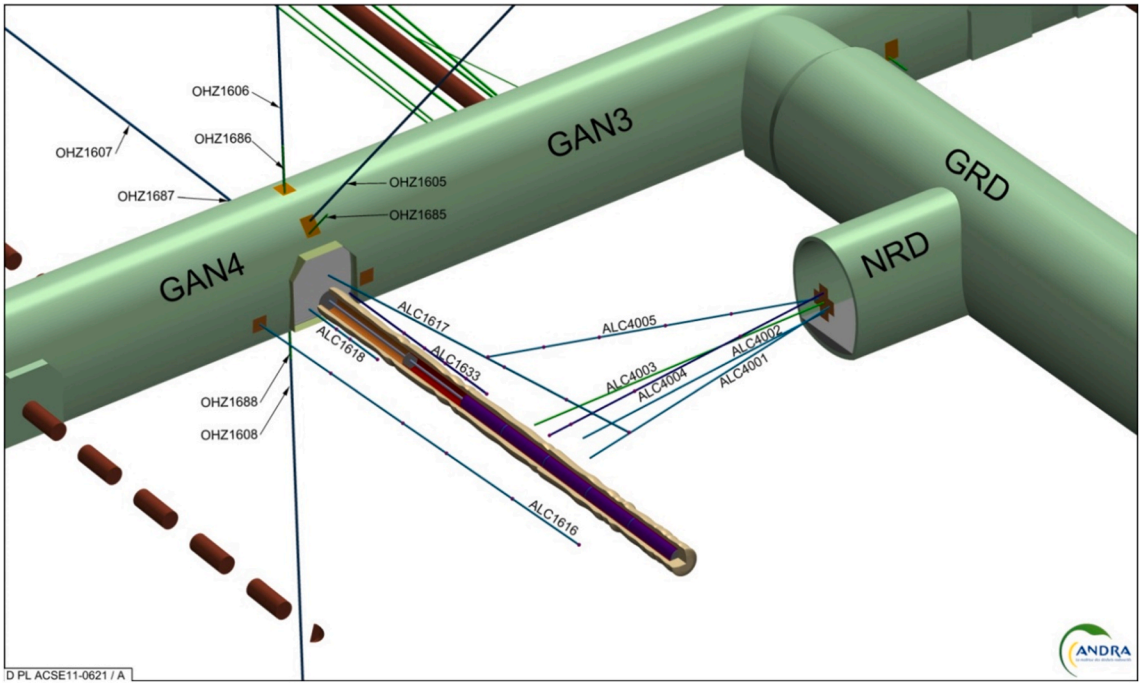

Fig. 3. General view of the peripheral instrumentation around ALC1604 cell.

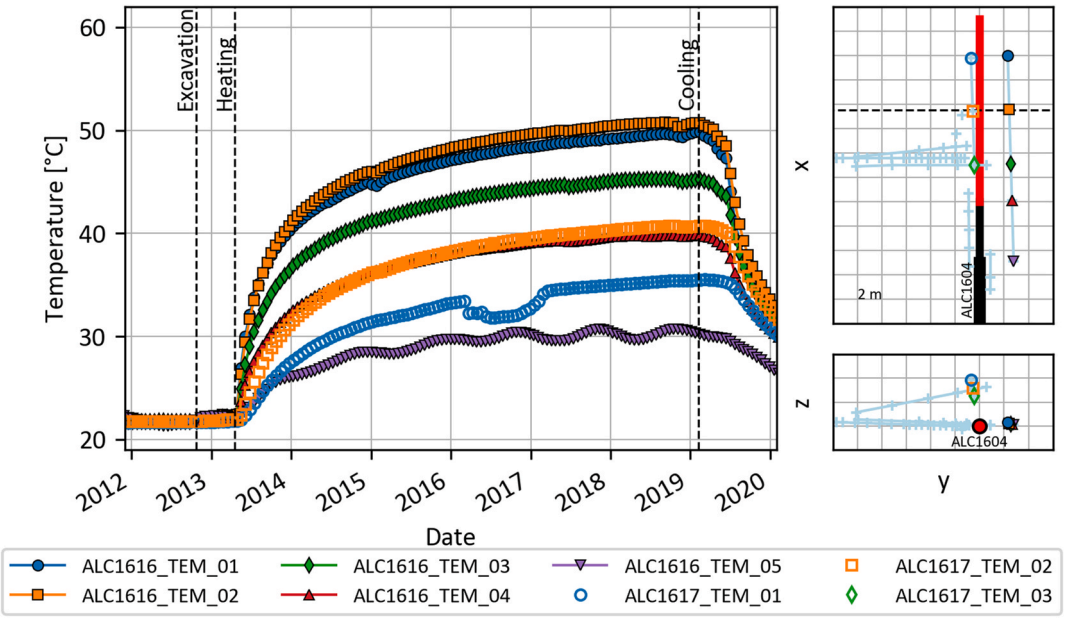

Fig. 4. Measurements of temperature evolution at sensors in ALC1616 (horizontal plane of the cell) and ALC1617 (vertical plane of the cell).

allow to study the temperature evolution in the COx during the heating phase. Similar tendency is observed in both directions and only the temperature at ALC1616_05 is affected by the temperature variation on the GAN drift wall. The temperature increased rapidly during the first year of the heating phase followed by a smooth increase that tended to stabilize over the last year, prior to the beginning of the cooling phase. As expected, the highest temperatures (approximately 50 °C) were recorded at the sensors located close to the mid-plane of the heated zone: ALC1616_01 and ALC1616_02 (1.9 m and 2 m from the cell wall, respectively). Despite the fact that the sensor ALC1617_02 was located at the mid-plane of the heated zone, it was 2.8 m far from the cell wall. Consequently, the maximum temperature in this sensor was about 40 °C.

The temperature evolution measured by the sensors installed in the peripheral boreholes ALC4005 and ALC1618 is shown in Fig. 5. The sensor ALC4005_05 did not record any measurement during the experiment. These measurements show additional points in intermediate locations to the bedding plane and show the temperature in the far field of the experiment which will be of help for the numerical analysis in order to better represent the temperature field in the rock mass (along with the pore pressure measurements). No measurements of temperature evolution monitored in ALC1618 (located near the drift wall) are recorded before October 23, 2012 since this borehole was drilled after the cell excavation. The effect of the beginning of the heating phase on the temperature is observed during the first year. Then, the temperature is strongly influenced by the seasonal temperature variation in the GAN drift, mainly in the two sensors located near the insert, i.e. the first 4 m from the drift wall, whereas the temperature evolution at ALC1618_01 is a combination of the drift temperature and the heating phase.

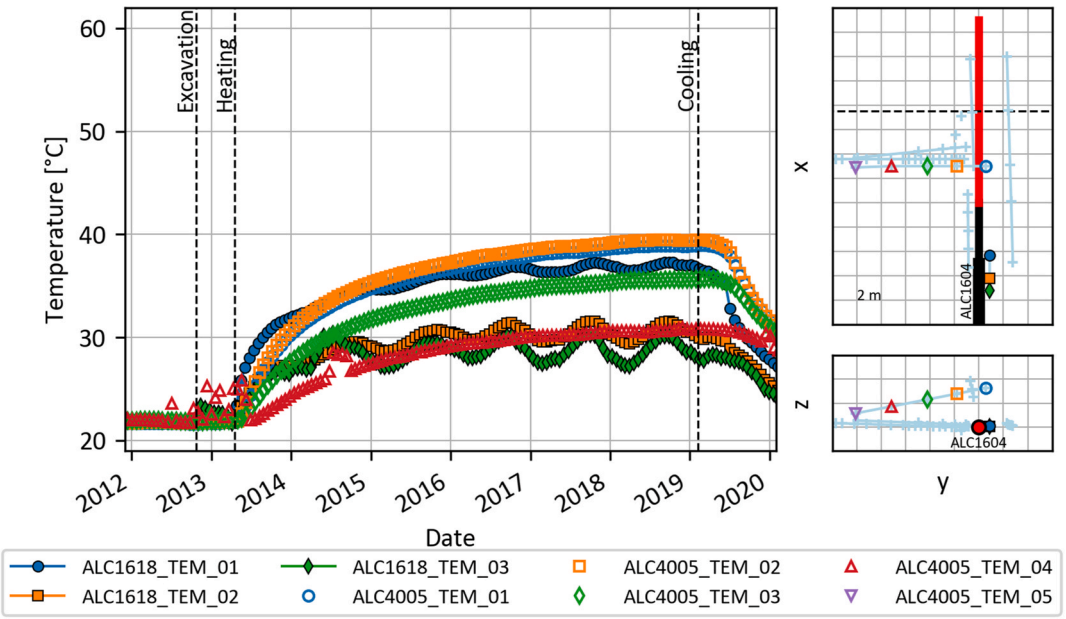

Fig. 5. Measurements of temperature evolution at sensors in ALC4005 and ALC1618.

4.2.2. Pore pressure

Fig. 6 shows the pore pressure evolution measured by the sensors in ALC1616 and ALC1617. The location of these two boreholes allows to study how the anisotropic properties of the COx affect its hydro-mechanical (HM) behavior during the cell excavation and THM behavior during the heating phase.

After the cell excavation, the measurements show a pore pressure increase in the horizontal plane and a pore pressure drop in the vertical plane. This behavior is scale independent since it has also been observed during 160 mm in diameter borehole drilling[3] and during 5 m in diameter drift excavation[16] both aligned with respect to the major horizontal stress. This anisotropic HM response to cell excavation is directly related to the anisotropy of the elastic stiffness of the rock mass as shown in Ref. 16.

The beginning of the main heating phase induced a pore pressure build-up in all sensors due to the difference between the thermal expansion coefficients of the pore water and of the rock. However, we observe a different behavior in the horizontal and vertical plane. The pore pressure achieved a maximum value of 7.5 MPa in ALC1616 three months after the beginning of the heating phase, followed by a rapid dissipation, whereas an overpressure peak of 8.3 MPa was reached in ALC1617 after three years of heating, followed by a slow dissipation. This different behavior observed in the boreholes located in the horizontal and vertical planes of the cell is in agreement with measurements made on former small-scale THM experiments at the MHM URL in which the anisotropic thermal and hydraulic properties of the rock play an important role such as lower permeability in the perpendicular direction to the bedding plane than in the parallel plane. The pore pressure evolution at ALC1616_05 located near the GAN drift experienced a slight increase due to the heating but, then, it was affected by its proximity to the drift wall and, consequently, by its seasonal temperature variation. The observed pore pressure drops in the sensor ALC1717_03 at 2.2 m from the cell wall two years after the cell excavation are related to a sealing failure in the packers insulating the chamber.

The thermal pressurization coefficient, which is calculated as the early slope of the linear part of the $\Delta P/\Delta T$ curve when heating began, was between 3 and 5 bar/°C, which is consistent with the value calculated for the TED experiment.[3]

4.3. Sleeve and insert

4.3.1. Thermal behavior

Fig. 7 shows the temperature evolution in the vault of the sleeve (solid lines) and the insert (dashed lines). In addition, the temperature evolution of the GAN drift is also shown. The impact of the heating system breakdowns was reduced by the fact that the other four heater elements functioned normally. The overall evolution of the sleeve temperature was therefore slightly affected and reached a maximum of 88 °C at the center of the heated zone after four years. Locally, however, the temperature dropped considerably between 8 and 15 °C at the sleeve intrados depending on the length of the cut-offs. As it was observed in the rock, the first 5 m where the head part of the cell is located, insert temperature evolution is affected by the temperature variation in the drift whereas the sleeve temperature in the first meters of the useable part is not.

Temperature profile on the lateral side of the sleeve is approximately 4 °C lower than that measured in the vault.[17] This difference can be explained both by convection occurring inside the sleeve and by the influence of the boundary conditions around the sleeve (the contact between the sleeve periphery and the rock is not homogeneous and is greater in the horizontal direction as explained in Section 4.3.3). In both cases, the highest temperature is located at a depth of approximately 18 m, i.e. at the center of the heated zone.

4.3.2. Hydric conditions in the cell

Relative humidity and temperature are measured in the annular space between the rock and the sleeve at different depths (Fig. 8). Before heating, relative humidity quickly reached 95% (almost as soon as the first measurements were taken, around 50 days after excavation). As expected, thermal loading results in sudden relative humidity decrease. The deepest sensor (21.5 m) was damaged when the heating began. The second-deepest sensor (17.5 m) also no longer functioned after recording resaturation (100%) after six months of heating. The other two sensors located in the annular space, at 13.5 m in the heated zone and 7.5 m outside the heated zone, have stabilized after slightly more than 2 years, at relative humidity between 86% and 70%, respectively. This evolution is the result of a balance being reached between the near field rock desiccation linked with the heating and water inflow linked with the rock being drained by the cell, the extent of which depends on

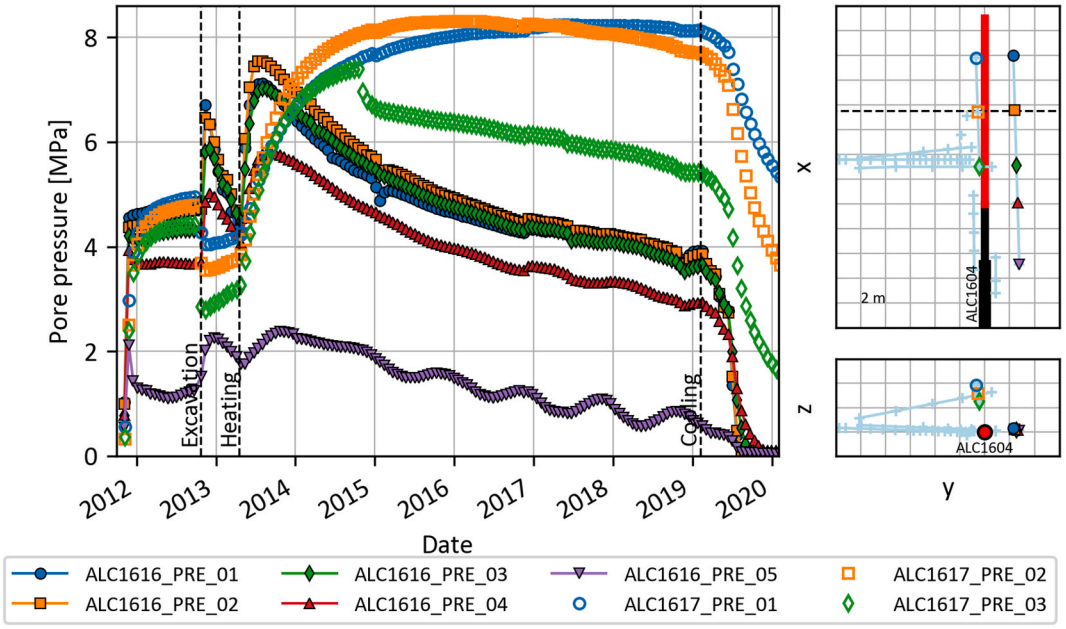

Fig. 6. Pore pressure evolution at boreholes ALC1616 (horizontal plane of the cell) and ALC1617 (vertical plane of the cell).

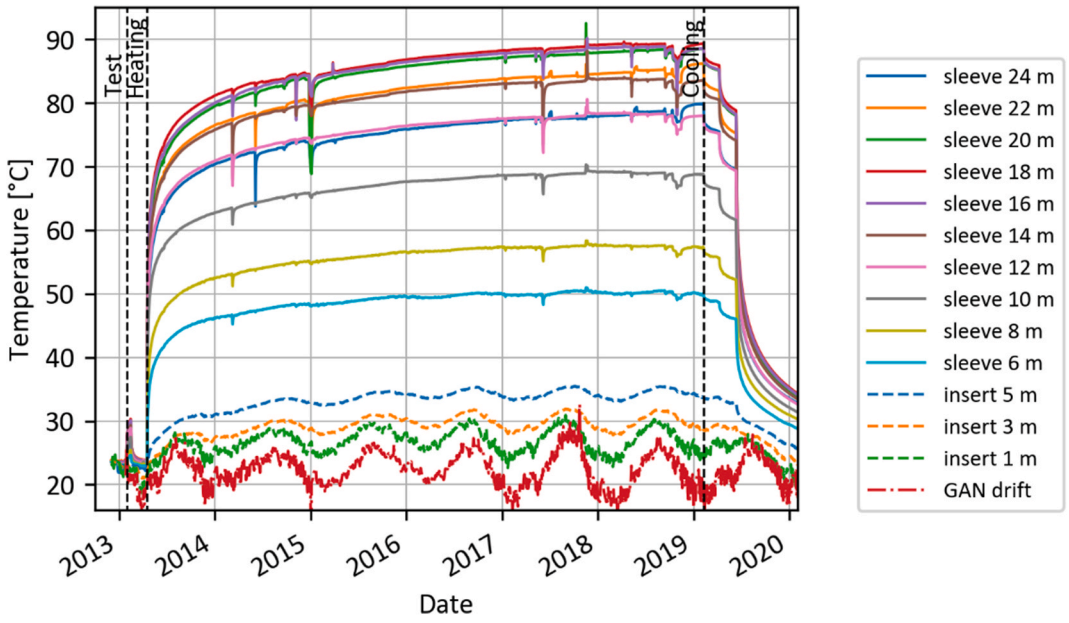

Fig. 7. Temperature evolution in the vault of the sleeve and the insert.

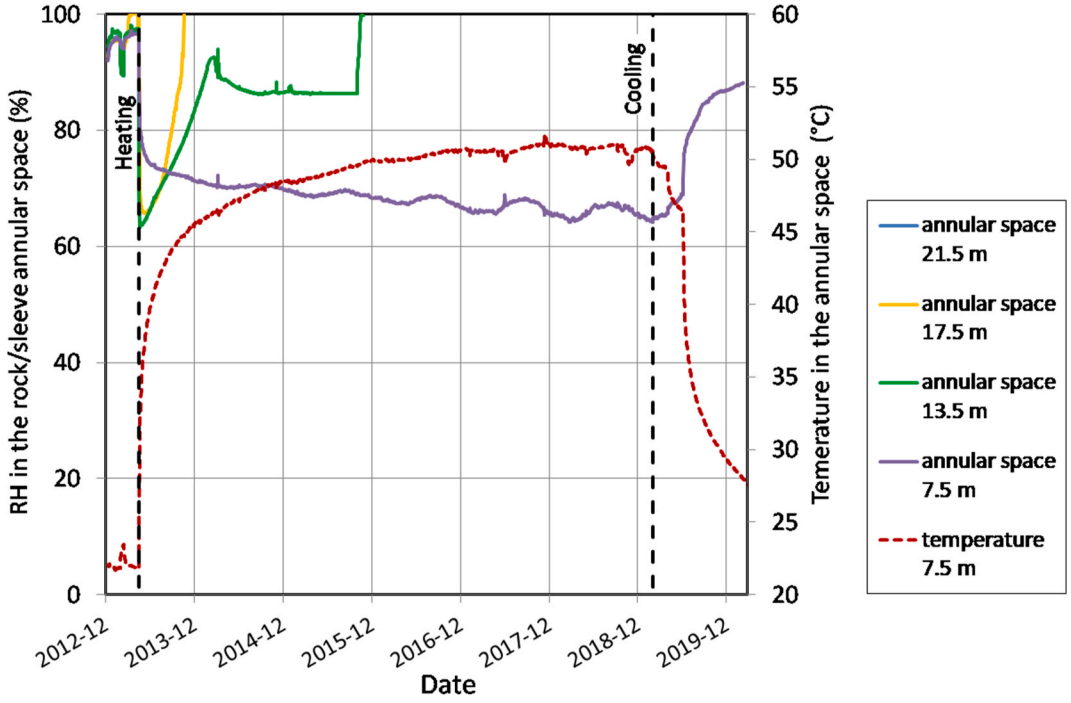

Fig. 8. Overall evolution of relative humidity in the annular space at different depths.

the hydraulic gradient and therefore the depth relative to the access drift. The sensor located at 13.5 m depth finally failed after 2.5 years of heating.

4.3.3. Sleeve and insert convergence

Due to the size of the heaters, no displacement sensors could be installed in the heated zone. The deepest convergence measurement section is located on sleeve element 9 at about 7 m depth. The evolution of the measurements is presented in Fig. 9.

As observed in previous in-situ experiments (see Section 2.2), an anisotropic convergence of the sleeve is observed before heating, as soon as the sensors were connected (i.e. 50 days after cell excavation). During this phase, radial loading is applied mainly along horizontal direction (the gap between the sleeve and the cell wall remains open in vertical direction) leading to a distortion of the sleeve into an oval shape. This behavior is directly related to the shape of the excavated damaged zone around the cell which is much more pronounced horizontally, thus inducing a greater convergence in the horizontal direction.

As observed on reduced scale heating test,[12] thermal loading results in an increase of radial loading and thus of the sleeve ovalization. Indeed it can be seen in Fig. 9, that the beginning of the heating phase considerably accelerated the sleeve convergence until the sleeve was in full contact with the cell vault 400 days after the cell was excavated. This phenomenon may be related to thermal expansion of the rock and to

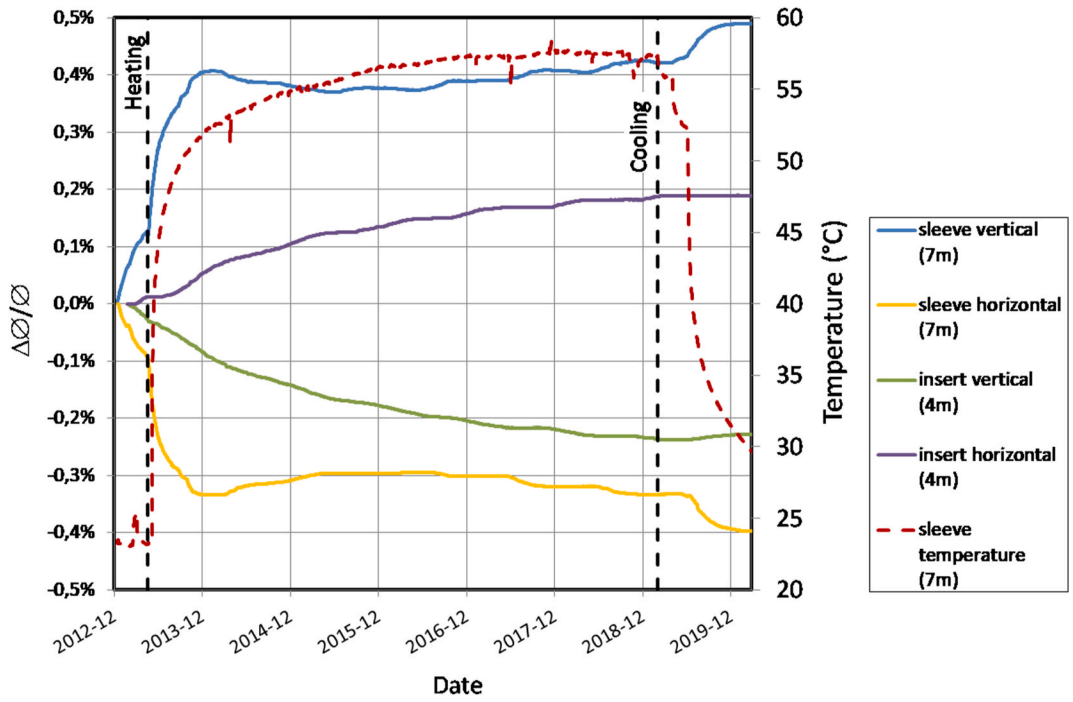

Fig. 9. Relative diameter variation measured on the sleeve and the insert.

creep rate increase of the rock with temperature. Temperature decrease during the cooling phase seems to result in a slight ovalization increase.

Two convergence measurement sections have also been installed on insert elements 11 and 12. They are not significantly affected by the heating phase due to their positions away from the heated zone. The loading schema is the reverse of that seen for the sleeve, consisting of vertical convergence and noticeably equivalent horizontal divergence (Fig. 9). Given that the annular space is much smaller at the insert level (initially 12 mm, compared with 25 mm around the sleeve), this behavior could be caused by the insert being in contact with the rock in the vertical and horizontal planes. As the mechanical strength of the rock was lower horizontally due to the damage generated during excavation, the insert tends to diverge horizontally. A similar behavior has been observed in more recent full-scale experiments in which the gap between the rock and the sleeve has been filled with a cement grout.[15] Mechanical loading of insert is also influenced by the surrounding stress field which has been modified by the GAN drift excavation.

4.3.4. Strain gauges measurements

Due to the absence of convergence measurement device, the thermomechanical behavior of the sleeve in the heating zone is only estimated from strain gauges measurements on the inner face at different angular positions. The mechanical signatures (i.e. evolution of the circumferential mechanical strain around the inner face of the sleeve) of the load applied to the sleeve at 14 and 18 m depth are presented in Fig. 10. In both cases the first curve (i.e. 2013-04) is the mechanical signature 2 weeks before the heating began. They are representative of a mainly horizontal loading of the sleeve and do not evolve significantly after 1 year of heating, meaning that ovalization of the sleeve is also quickly blocked in the heated zone.

The axial gauges generally only show small mechanical deformations of less than 150 μm/m which can partly be explained by the sliding of the sleeve (see next section) in the insert, thereby reducing the axial compression stress of the sleeve.

4.3.5. Sleeve sliding in the insert

The sliding of the sleeve in the insert vary between 2.6 and 2.7 mm at the lower part of the sleeve, and 4.2 mm at the vault. This difference could partly be due to an axial bending of sleeve element n°10. However, the sliding remains below the free thermal elongation of the sleeve for the corresponding temperature rise, which should be of the order of 10 mm meaning that part of the sleeve elongation is towards the bottom

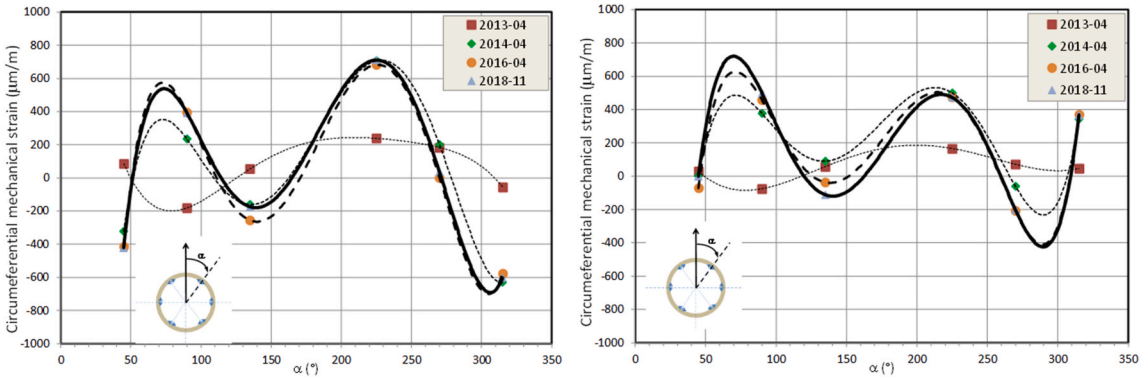

Fig. 10. Time evolution of the mechanical signature of the loading at 14 m (left) and 18 m (right).

of the cell.

5. Numerical simulation

5.1. Numerical models

Two numerical models were used for the reproduction of the THM behavior of the COx due to cell excavation and heating.

The first numerical model was performed by Andra as part of Task E of the DECOVALEX-2019 project.[18] Its theoretical formulation is based on the general expression of the governing equations for a classical thermo-poro-elastic saturated medium as developed in Ref. 19. The anisotropy induced by the bedding is taken into account by considering a transversely isotropic elastic stiffness tensor in the mechanical law as well as in the thermal conductivity and saturated permeability tensors. The numerical code used for the numerical analysis was COMSOL Multiphysics® and its objective was the prediction of the THM response of the COx in the heating phase by using the parameters obtained from the model calibration of the small-scale TED experiment performed within Task E.

The second numerical model was developed at Universitat Politècnica de Catalunya (UPC).[20–22] Its theoretical formulation is based on using multi-phase, multi-species approach to porous medium modelling.[23] It is assumed that the porous medium is composed of three species: mineral, water and air, distributed in three phases: solid, liquid and gas. The mechanical behavior is modelled with a cross-anisotropic elastoplastic model extended to consider creep effects as described in Ref. 24,25. In addition, the intrinsic permeability incorporates a dependency on the plastic multiplier of the elastoplastic model to reproduce the large increase of permeability when the rock experiences damage. The numerical analysis was performed with CODE_BRIGHT[26] and its objective was to reproduce the experimental measurements: pore pressure, temperature in the COx, thermomechanical behavior of the sleeve/insert. Unlike the previous model, some parameters were back analyzed.

Andra assumed that the thermal response was uncoupled from the hydro-mechanical behavior. This assumption holds true in the far field were the host rock is not damaged and heat convection could be neglected due to the low permeability of the COx.[27] UPC's THM formulation is fully coupled. In that way, convection processes occurring in the EDZ and in the gap are taken into account. Furthermore, the water properties are expressed as functions of the temperature and pore pressure.[18]

The model used the local axis system that was defined for the ALC experiment; its origin (0,0,0) is the head of ALC1604. The x-axis coincides with the cell axis and the y-axis coincides with the GAN drift axis. The domain consists of a cube with a side length of 50 m; this geometry corresponds to the distance between the cell and the GRD drift and is considered large enough regarding the diameter of the ALC1604 cell. The cube is centered at height z = 0. Andra represented half of the GAN drift (radius = 2.6 m) and half of the GRD drift (radius = 2.85 m), in such a way that one face of the cube coincides with the plane x = −2.6 m and another face coincides with the plane y = 21.6 m. Thus, the cube coordinates vary between x = −2.6 m to 47.4 m, y = −28.4 m to 21.6 m, and z = −25 m to 25 m. UPC did not explicitly represent the drifts but their THM influence was considered by the imposed boundary conditions on the zones where they were supposed to be. The geometries of both models with their respective finite element meshes are presented in Fig. 11.

The presence of the sleeve, the insert, and the annular space was not considered by Andra whereas UPC's model included these three components. The steel sleeve/insert is considered to be linear elastic. The annular space was modelled as an unsaturated continuous medium that considers the gap closure through its property evolution from a highly porous medium with air properties to host rock properties. Therefore, its retention curve is given by a reference air entry capillarity pressure, P_0, as the gap is in essence a material with very large pores. Dependency of both permeability and air entry pressure on porosity was considered in order to model their evolution towards host rock values when the gap closes. The mechanical behavior of the gap was modelled using a bilinear elastic model to represent, first, the open gap and, then, the contact with the rock mass. The volumetric strain was used to check whether the gap was open or closed. Andra modelled the excavation damaged zone (EDZ) of 1 m thick around the drifts with a constant higher permeability ($\sim 10^{-15}$ m^2).

The simulation starts with an initialization step before the excavation of the GAN and GRD/NRD drifts. The initial stress state at experiment level was given as follows: the major principal total stress, $\sigma_H = -16.1$ MPa, coincides with σ_x, the minor principal total stress, $\sigma_h = -12.4$ MPa, with σ_y, and the intermediate principal total stress, $\sigma_v = -12.7$ MPa, is oriented in the z direction. The initial pore pressure is equals to 4.7 MPa. The temperature is 22.0 °C. The GAN drift was excavated in several phases from November 3, 2009 to February 6, 2012. The drift-face passed by the ALC1604 location on May 3, 2011. The first 27 m of the GRD drift close to the GAN drift were excavated from December 16, 2010 to April 7, 2011. The numerical model set the initial time on October 23, 2012, corresponding to the beginning of the cell excavation. Andra simulated only the first 4 years of the measurements and the cooling phase was considered only by UPC.

Regarding the boundary conditions, all instrumentation boreholes can be considered watertight except the extensometer borehole ALC4004 which was shown to be draining and was modelled by Andra. Since the annular space of the ALC1604 was not backfilled, the cell was also considered draining. The temperature evolution in the GAN and GRD drifts, atmospheric pressure and a normal stress of 0.3 MPa were applied on the drift walls.

No heat flux was imposed prior to the heating phase. The heaters were emitting less heat than the designed heater output according to the

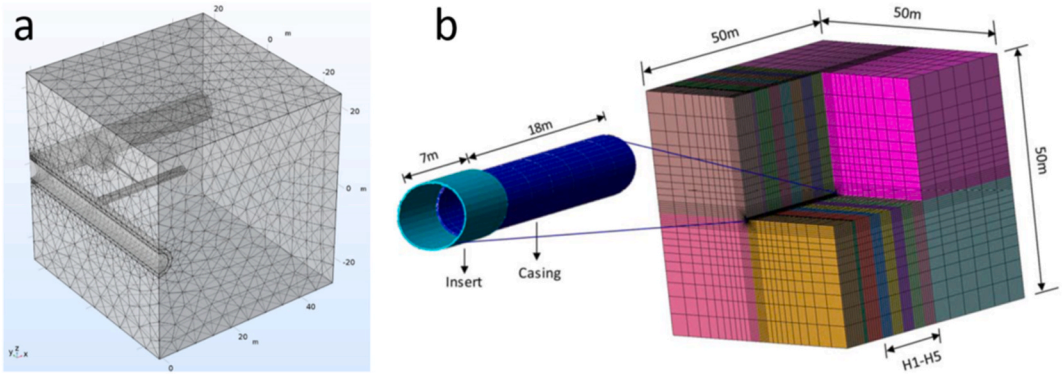

Fig. 11. Andra's (a) and UPC's (b) model geometry and finite element mesh for the numerical simulation of the ALC1604 experiment.

observed temperature measurements. Therefore, Andra considered a 95% of the total heating power emitted from the heaters. UPC applied on the non-heated zone a small part of the heating power (11%) removed from the heated zone (89%). This was an approximate way to consider the conduction/radiation and air convection processes occurring in the non-heated zone. The heat flux values used were obtained by a trial-error procedure based on the comparison between computed and measured temperature profiles.

The THM parameters of the thermo-poro-elastic model are listed in Appendix A1 and the parameters of the UPC's model (the material parameters of the COx, the steel sleeve/insert and the gap) are given in Appendix A2.

5.2. Surrounding rock

5.2.1. Temperature

Fig. 12 shows the comparison of the measurements and the Andra and UPC's numerical results of the temperature evolution at two sensors in boreholes ALC1616, ALC1617, and ALC4005. Andra's numerical results are represented with dashed lines, UPC's numerical results with solid lines and the measurements with squares. The numerical results in these three boreholes intend to be representative of the anisotropic thermal response of the COx. The numerical results show a good agreement with the measurements. Andra's results show an overestimation on the sensors located in the heated zone (ALC1616_02, ALC1617_01, ALC1617_02, and ALC4005_02), whereas the UPC's results show a slight underestimation (ALC1616_02). On the other hand, Andra's results underestimate the temperature on the sensors located in the non-heated zone (ALC1616_05, ALC4005_04), whereas the UPC's results show a perfect match. This can be explained by the different thermal boundary conditions of the cell employed by Andra and UPC. Approximating the conduction/radiation and air convection processes by adding a small part of the heating power proved to be a good approximation in combination with the assumption of power losses. Furthermore, the temperature oscillations due to the seasonal temperature variation on the drift walls are well reproduced by the geometry simplification of the drifts in UPC's model as well as by the explicitly representation of the drifts in Andra's model.

The anisotropic thermal parameters in both models (see Appendix) are in accordance with the values given in Table 1 and with former small-scale THM experiments.[3,28]

5.2.2. Pore pressure

The comparison of the measurements of the pore pressure and the numerical results are presented in Fig. 13 for Andra and for UPC. The results are given for boreholes ALC1616 and ALC1617. The numerical results of the cell excavation show as anticipated, that the poro-elastic approach was not able to reproduce the anisotropic HM response observed in the measurements and discussed in Section 4.2.2 whereas the UPC's model captured this effect reasonably well. Variation of pore pressure during the excavation reflects the volumetric deformation change in undrained conditions due to the low permeability of the rock mass. It has been shown in Ref. 11 that excavation in COx induces large deformation and damage up to fracture opening. Poro-elastic approach underestimated volumetric deformation during excavation whereas UPC elasto-visco-plastic model better represented rock mass deformation. These overpressures and pressure drops can be observed in a zone further away, i.e. up to 4 cell diameters in this case. Also the modifications of the hydraulic properties due to the dependency on damage play an important role and they are accounted for in the UPC's model. Globally, the pore pressure field before the heating phase is better reproduced with the anisotropic elasto-visco-plastic model (anisotropy in stiffness and strength); the thermo-poro-elastic approach obtained higher values in the perpendicular direction to the bedding (ALC1617_01 and ALC1617_02).

The THM response of the COx due to the heating phase is well represented in the horizontal plane of the cell (ALC1616_02), although Andra only reproduced the pore pressure build-up. The slow dissipation of the pore pressure in the perpendicular direction was only captured by the anisotropic elasto-visco-plastic model (ALC1617_01 and ALC1617_02). The fact that the changes in the hydraulic properties are not considered in the thermo-poro-elastic approach could be an explanation. However, the EDZ is reduced in the vertical direction since the cell is excavated along the major stress direction.[29] So, this may be due to the pore pressure field around the cell prior to the heating phase where the numerical pore pressure is higher than the measurements

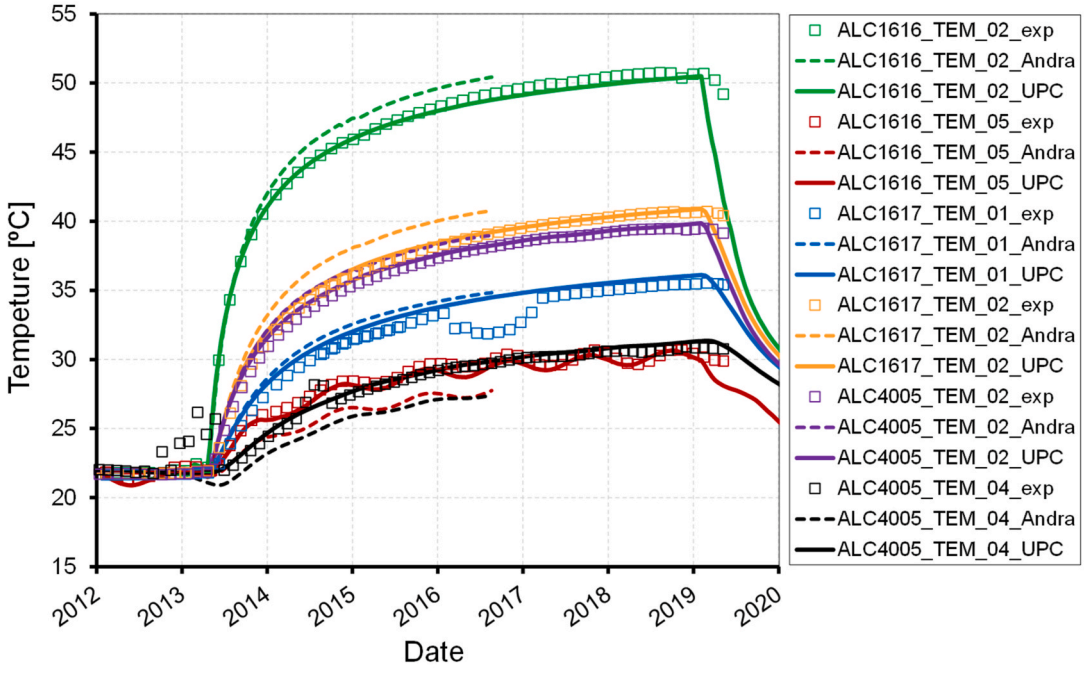

Fig. 12. Comparison of Andra and UPC's numerical results and measurements of temperature evolution at sensors in boreholes ALC1616, ALC1617 and ALC4005.

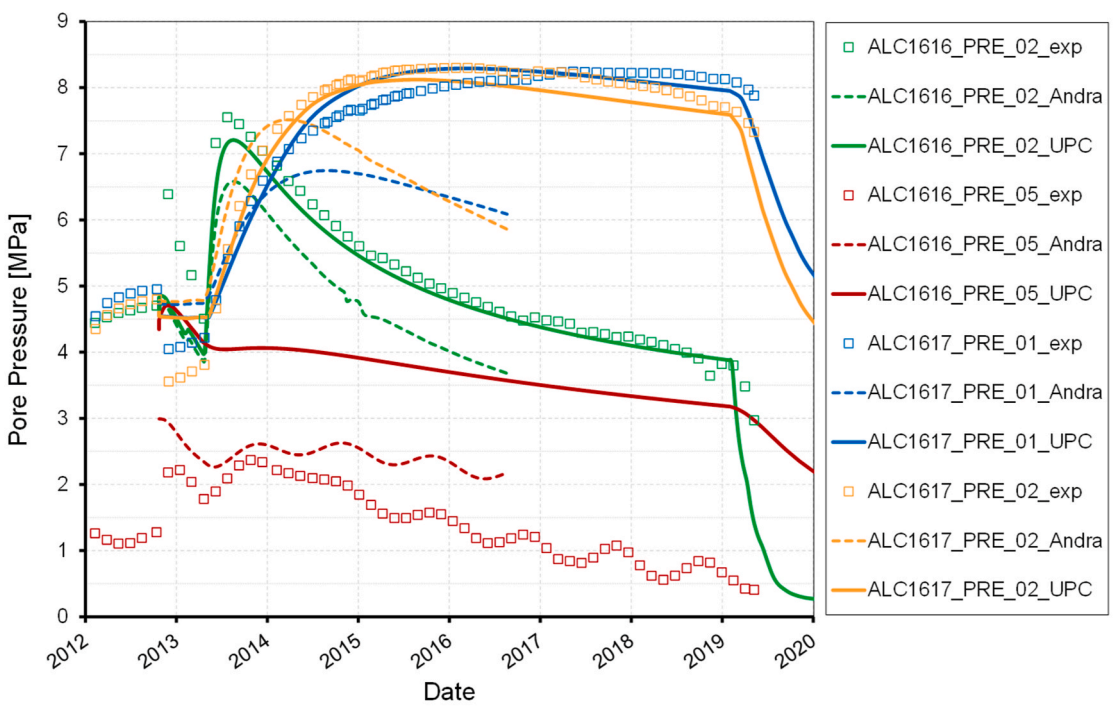

Fig. 13. Comparison of Andra and UPC's numerical results and measurements of pore pressure evolution at sensors in boreholes ALC1616 and ALC1617.

where a slight pore pressure recovery is observed. In the numerical pore pressures, the dissipation process may be accelerated by the difference in the pore pressure gradients occurring in the heated zone. Finally, the fact that the UPC back-analyzed some model parameters could also help to obtain a better reproduction. As a remainder, in the case of Andra, the model parameters were obtained from the small-scale experiment TED, and were not changed during this study, ignoring the spatial variability in the COX properties. One of the differences in the common parameters of both models were found in the anisotropy ratio of the permeability, 4 and 2 for Andra and UPC, respectively. Nevertheless, the main HM parameters used in both models were in the range of the values given in Table 1.

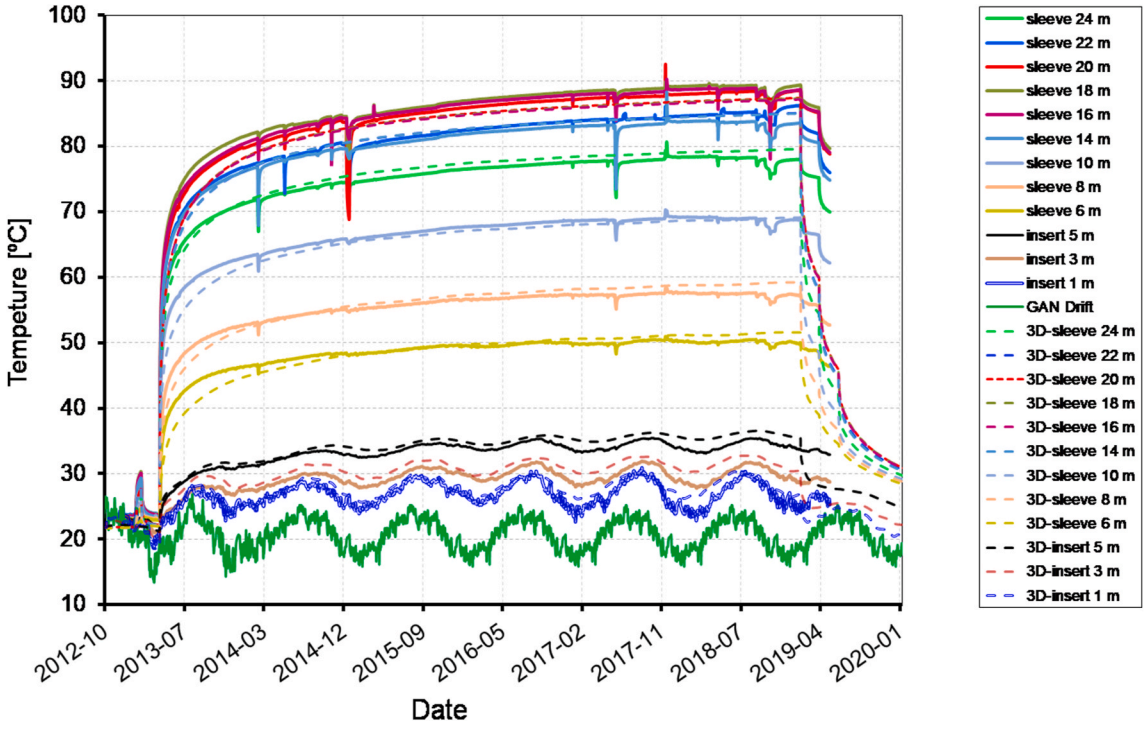

Fig. 14. Comparison of UPC's numerical results and measurements of temperature of the sensors at the vault of the sleeve and the insert.

5.3. Sleeve and insert

5.3.1. Thermal behavior

Fig. 14 shows the comparison of the numerical results and the measurements of the temperature at the vault of the sleeve/insert. The measurements are represented with solid lines and the numerical results with dashed lines. A good agreement can be observed for all the measurements. This confirms that the convective and radiation processes occurring inside the sleeve/insert cannot be neglected for the correct reproduction of the TM behavior of the sleeve/insert. Therefore, the heat flow assumed in the non-heated zone is a good approximation.

5.3.2. Sleeve and insert convergence

The numerical results (solid and dashed lines) of the sleeve and insert convergence are shown in Fig. 15 along with the measurements (diamonds). The numerical results show a good reproduction of the measurements in the two sections. Modelling the gap between the sleeve and the rock with bi-linear joint elements leads to a good reproduction of the maximum convergence of sleeve element n°9 (at 7 m from the access drift), meaning that the kinetics of vertical gap decrease is well captured by the model. The influence of the thermal loading is slightly underestimated.

The reversal of ovalization direction of insert element n°11 (at 4 m from the access drift, almost not influenced by the heating) in comparison to that of the sleeve, is well reproduced. Since the excavation of the GAN drift is not modelled, the reproduction of this phenomenon is only due to the fact that the initial gap around the insert is thinner than around the sleeve and the contact at the vault of the insert occurs at a very early stage.

6. Conclusion

ALC1604 experiment has demonstrated the construction feasibility of a full-scale (in terms of diameter) HLW disposal cell including head and useable parts as originally designed. The extensive instrumentation set-up of this first full-scale heating experiment performed at the MHM URL led to a better understanding of the THM behavior of the disposal cell and the surrounding rock.

Concerning the THM behavior of the COx claystone, the experiment provided new data on the HM response to a micro-tunnel excavation that are fully consistent with previous in-situ experiments, at all scales. It highlighted the anisotropy of short-term pore pressure evolution mainly governed by the anisotropy of elastic moduli of the COx claystone and the deepness in the rock wall where the pore pressure field is affected by the excavation. It also emphasized that elasto-visco-plastic models are more accurate than poro-elastic model to model excavation in this type of claystone.

The influence of a thermal loading on the pore pressure is also consistent with previous small-scale experiments. After a pressure increase, due to the difference between the thermal expansion coefficients of pore water and solid skeleton, overpressures dissipate with a kinetics governed by anisotropic hydraulic properties of the rock. The behavior during the heating phase is nearly elastic as it is shown by the satisfactorily prediction of the thermo-poro-elastic model taking into account anisotropic parameters in accordance with values identified from back analysis of former small-scale heating experiments and laboratory tests. However, pore pressure field evolution is better reproduced with a time-dependent anisotropic elastoplastic THM model than with an anisotropic thermo-poro-elastic approach mainly because the initial (after excavation) pore pressure field and the modifications of the hydraulic properties due to the dependency on damage in the damage zone, gives a better description of in-situ observations. Concerning the mechanical behavior of the steel sleeve, it is subjected to anisotropic loading from its emplacement in the micro-tunnel. This behavior is directly related to the anisotropy of the excavation-induced fracture network around the cell and leads to the sleeve ovalization. The radial loading increases with temperature due to rock thermal expansion resulting in an increase of the convergence rate of the sleeve until it reaches the vault of the cell. First simulations of the mechanical behavior of the sleeve are quite encouraging since the anisotropic loading seems to be satisfactorily reproduced.

ALC1604 experiment also provided valuable feedback towards

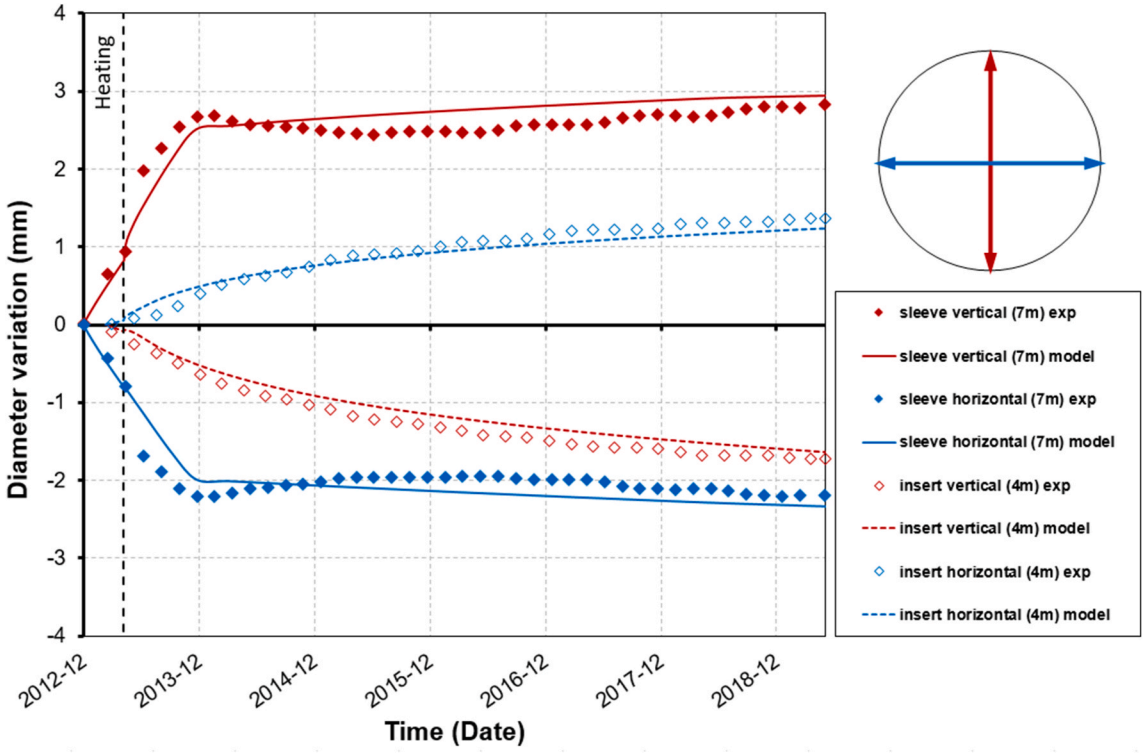

Fig. 15. Comparison of numerical results and measurements of diameter variation of sleeve and insert.

implementing new full-scale heating experiments consistent with the benchmark concept optimization.

Declaration of competing interest

The authors declare that they have no known competing financial interests or personal relationships that could have appeared to influence the work reported in this paper.

Acknowledgements

DECOVALEX is an international research project comprising participants from industry, government and academia, focusing on development of understanding, models and codes in complex coupled problems in sub-surface geological and engineering applications; DECOVALEX-2019 is the current phase of the project. The authors appreciate and thank the DECOVALEX-2019 Funding Organizations Andra, BGR/UFZ, CNSC, US DOE, ENSI, JAEA, IRSN, KAERI, NWMO, RWM, SÚRAO, SSM and Taipower for their financial and technical support of the work described in this report. The statements made in the report are, however, solely those of the authors and do not necessarily reflect those of the Funding Organizations.

The experimental work presented in this article has received funding from the European Atomic Energy Community's Seventh Framework Program under Grant Agreement n◦269905, the LUCOEX project. The financial support is gratefully acknowledged.

Appendix A.1

Table 2
Thermo-poro-elasticity parameters.

Parameter	Unit	Symbol	Value
Young's modulus parallel to bedding	Pa	E_{yh}	8.0×10^9
Young's modulus perpendicular to bedding	Pa	E_{yv}	5.0×10^9
Poisson's ratio horizontal plane	–	ν_{hH}	0.3
Poisson's ratio vertical planes	–	ν_{hv}	0.3
Intrinsic permeability parallel to bedding	m^2	K_h	2.5×10^{-20}
Intrinsic permeability perpendicular to bedding	m^2	K_v	0.6×10^{-20}
Thermal conductivity parallel to bedding	W/m/K	λ_h	1.97
Thermal conductivity perpendicular to bedding	W/m/K	λ_v	1.29
Linear thermal expansion coefficient of solid grains	K^{-1}	α_T	1.4×10^{-5}
Specific heat capacity of solid grains	J/kg/K	C_{ps}	800.0
Biot coefficient	–	b	0.6
Solid compressibility	Pa^{-1}	β_s	2.5×10^{-5}
Specific weight of solid grains	kg/m^3	ρ_s	2.6
Porosity	–	Φ	0.15

Appendix A.2

Parameters of UPC's model

Table 3
Mechanical parameters of the time-dependent anisotropic model.

Parameter	Unit	Symbol	Value
Young's modulus parallel to bedding	Pa	E_{yh}	5.2×10^9
Young's modulus perpendicular to bedding	Pa	E_{yv}	4.0×10^9
Poisson's ratio horizontal plane	–	ν_{hH}	0.25
Poisson's ratio vertical plane	–	ν_{hv}	0.35
Peak friction angle	◦	φ_{peak}	22.0
Initial friction angle	◦	φ_{ini}	9.35
Mobilized friction angle	◦	φ_{res}	14.74
Peak cohesion	Pa		3×10^6
Constant that controls the curvature of the function in the hardening branch	–	a_{hard}	0.0035
Constant that controls the curvature of the function in the softening branch	–	a_{soft}	0.07
Coefficient of non-associativity	–	ω	0.6
Equivalent plastic strain at which the maximum strength is reached	Pa	ξ_1	5.0×10^3
Equivalent plastic strain at which softening begins	Pa	ξ_2	6.0×10^3
Equivalent plastic strain at which the residual strength is reached	Pa	ξ_3	6.0×10^4
The threshold from which creep strains are activated	Pa	σ_s	4.0×10^6
Viscosity parameter	day^{-1}	γ	1.0×10^{-7}
Exponent of stress deviatoric term in the creep law	–	n	3.37
Exponent of creep strain term in the creep law	–	m	530

Table 4
Hydraulic parameters.

Parameter	Unit	Symbol	Value
Intrinsic permeability parallel to bedding	m^2	K_h	2.0×10^{-20}
Intrinsic permeability perpendicular to bedding	m^2	K_v	1.0×10^{-20}
Material parameters controlling the change of hydraulic conductivity with degree of saturation	–	A	1.0
	–	Λ	3.0
Material parameters controlling the shape of the retention curve	Pa	P	1.43×10^7
	–	λ	0.33

Table 5
Coupling parameters.

Parameter	Unit	Symbol	Value
Linear thermal expansion coefficient of the rock	K^{-1}	α_T	1.4×10^{-5}
Biot coefficient	–	b	0.6
Constant that controls the rate of change of intrinsic permeability with equivalent plastic strain	–	η	10
Solid compressibility	Pa^{-1}	β_s	2.5×10^{-5}
Specific weight of solid grains	kg/m^3	ρ_s	2.7
Porosity	–	Φ	0.173

Table 6
Thermal parameters for the COx.

Parameter	Unit	Symbol	Value
Thermal conductivity parallel to bedding	W/m/K	λ_h	2.05
Thermal conductivity perpendicular to bedding	W/m/K	λ_v	1.33
Linear thermal expansion coefficient of solid grains	K^{-1}	α_T	1.4×10^{-5}
Specific heat capacity of solid grains	J/kg/K	C_{ps}	800.0

Table 7
Thermo-mechanical parameters for the sleeve/insert.

Parameter	Unit	Symbol	Value
Thermal conductivity	W/m/K	λ_{steel}	80.0
Specific heat	J/kg/K	C_{psteel}	550
Linear thermal expansion coefficient	K^{-1}	α_{Tsteel}	1.4×10^{-5}
Young's modulus	MPa	E_{steel}	180×10^3
Poisson's ratio	–	ν	0.3

Table 8
Thermo-hydro-mechanical parameters for the gap.

Parameter	Unit	Symbol	Value
Thermal conductivity in saturated conditions	W/m/K	$\lambda_{sat,gap}$	0.035
Thermal conductivity in dry conditions	W/m/K	$\lambda_{dry,gap}$	0.6
Specific heat	J/kg/K	C_{pgap}	1100.0
Intrinsic permeability	m^2	K_{gap}	1.0×10^{-16}
Porosity	–	Φ_0	0.8
Parameter for van Genuchten model	–	λ	0.5
Air entry capillarity pressure (P_0)	Pa	P_0	1.0×10^3
$P_0(\Phi) = P_0 \exp[\alpha(\Phi_0 - \Phi)]$	–	α	10
Young's modulus (closed gap)	Pa	E_c	1.0×10^9
Young's modulus (open gap)	Pa	E_0	1.0×10^6
Strain limit	–	ε_{vlimit}	0.005
Poisson's ratio	–	ν	0.3

References

1 Mohajerani M, Delage P, Sulem J, Monfared M, Tang AM, Gatmiri B. A laboratory investigation of thermally induced pore pressure in the Callovo-Oxfordian claystone. *Int J Rock Mech Min Sci.* 2012;52:112–121.

2 Conil N, Armand G, Garitte B, et al. In situ heating test in Callovo-Oxfordian claystone: measurement and interpretation. Montpellier. In: *Proceedings of 5th Int. Conf. On Clays in Natural and Engineered Barriers for Radioactive Waste Confinement.* October 2012:22–25.

3 Conil N, Vitel M, Plúa C, Vu MN, Seyedi D, Armand G. In situ investigation of the THM behavior of the callovo-oxfordian claystone. *Rock Mech Rock Eng.* 2020;53:2747–2769.

4 Seyedi D, Armand G, Conil N, Vitel M, Vu MN. On the thermo-hydro-mechanical pressurization in callovo-oxfordian claystone under thermal loading. *Poromechanics VI: Proceedings of the Sixth Biot Conference on Poromechanics.* 2017:754–761.

5 Vu MN, Armand G, Plua C. Thermal pressurization coefficient of anisotropic elastic porous media. *Rock Mech Rock Eng.* 2020;53:2027–2031.

6 Karamanos SA, Sarvanis GC, Keil BD, Card RJ. Analysis and design of buried steel water pipelines in seismic areas. *J Pipeline Syst Eng Pract.* 2017;8(4).

7 Bosgiraud JM, Baroux C, Bumbieler F, Crusset D. *HLW disposal package for cigéo: design basis and development timeline. Proceedings of 16th International High-Level Radioactive Waste Management Conference.* Charlotte; 9-13 April 2017:52–61.

8 Necib S, Linard Y, Crusset D, et al. Corrosion at the carbon steel–clay borehole water and gas interfaces at 85°C under anoxic and transient acidic conditions. *Corrosion Sci*. 2016;111:242–258.
9 Wileveau Y, Cornet FH, Desroches J, Blumling P. Complete in situ stress determination in an argillite sedimentary formation. *Phys Chem Earth*. 2007;32:866–878.
10 Robinet JC, Sardini P, Coelho D, et al. Effects of mineral distribution at mesoscopic scale on solute diffusion in a clayrich rock: example of the Callovo-Oxfordian mudstone (Bure, France). *Water Resour Res*. 2012;48(5):17–27.
11 Armand G, Noiret A, Zghondi J, Seyedi D. Short- and long-term behaviors of drifts in the callovo-oxfordian claystone at the meuse/haute-marne underground research laboratory. *Journal of Rock Mechanics and Geotechnical Engineering*. 2013;5:221–230.
12 Armand G, Bumbieler F, Conil N, de la Vaissière R, Bosgiraud JM, Vu MN. Main outcomes from in situ thermo-hydro-mechanical experiments programme to demonstrate feasibility of radioactive high-level waste disposal in the Callovo-Oxfordian claystone. *Journal of Rock Mechanics and Geotechnical Engineering*. 2017;9(3):415–427.
13 Delay J, Vinsot A, Krieguer JM, Rebours H, Armand G. Making of the underground scientific experimental programme at the meuse/haute-marne underground research laboratory, north eastern France. *Phys Chem Earth*. 2007;32:2–18.
14 Morel J, Renaud V, Armand G. Feasibility of excavation of disposal cells in 500 m deep clay formation. Rock Engineering in difficult ground conditions – soft rocks and karst. *Proceedings of EUROCK*. 2009:561–566.
15 Bumbieler F, Armand G. *In-situ characterization of mechanical loads applied on a deep-buried steel casing. Proceedings of 2nd International Conference on Natural Hazards & Infrastructure*. Chania; 23 – 26 June 2019.
16 Guayacán-Carrillo LM, Ghabezloo S, Sulem J, Seyedi D, Armand G. Effect of anisotropy and hydro-mechanical couplings on pore pressure evolution during tunnel excavation in low-permeability ground. *Int J Rock Mech Min Sci*. 2017;97:1–14.
17 Gugala J. Final report LUCOEX – WP3. D3:04 https://igdtp.eu/activity/lucoex-large-underground-concept-experiments/; 2015.
18 Seyedi D, Plúa C, Vitel M, et al. Upscaling THM modelling from small-scale to full-scale in-situ experiments in the Callovo-Oxfordian claystone. (Submitted in IJRMMS).
19 Coussy O. *Poromechanics*. Wiley; 2004.
20 Tourchi S, Vaunat J, Gens A, Vu MN, Bumbieler F. *Coupled THM analysis of long-term anisotropic convergence in the full-scale micro tunnel excavated in the callovo-oxfordian argillite*. Barcelona. In: *Proceedings of VIII International Conference on Coupled Problems in Science and Engineering (COUPLED PROBLEMS 2019)*. 3-5 June, 2019.
21 Tourchi S, Vaunat J, Gens A, Vu MN, Bumbieler F. *Thermo-Hydro-Mechanical simulation of a full-scale steel-lined micro-tunnel excavated in the Callovo-Oxfordian Argillite*. Barcelona. In: *Proceedings of XIV International Conference on Computational Plasticity. Fundamentals and Applications (COMPLAS 2019)*. 3-5 September, 2019.
22 Tourchi S, Vaunat J, Gens A., Bumbieler F, Vu MN, Armand G. A full-scale in situ heating test in Callovo-Oxfordian claystone: observations, analysis and interpretation. (Submitted in Computers and Geotechnics).
23 Olivella S, Carrera J, Gens A, Alonso EE. Non isothermal multiphase flow of brine and gas through saline media. *Transport Porous Media*. 1994;15(3):271–293.
24 Mánica M, Gens A, Vaunat J, Ruiz DF. A cross-anisotropic formulation for elasto-plastic models. *Géotech Lett*. 2016;6(2):156–162.
25 Mánica M, Gens A, Vaunat J, Ruiz DF. A time-dependent anisotropic model for argillaceous rocks. Application to an underground excavation in callovo-oxfordian claystone. *Comput Geotech*. 2017;85:341–350.
26 Olivella S, Gens A, Carrera J, Alonso EE. Numerical formulation for a simulator 'CODE_BRIGHT' for the coupled analysis of saline media. *Eng Comput*. 1996;13(7):87–112.
27 Gens A, Vaunat J, Garitte B, Wileveau Y. In situ behaviour of a still layered clay subject to thermal loading: observations and interpretation. *Geotechnique*. 2007;57:207–228.
28 Garitte B, Gens A, Vaunat J, Armand G. Thermal conductivity of argillaceous rocks: determination methodology using in situ heating tests. *Rock Mech Rock Eng*. 2014;47:111–129.
29 Armand G, Leveau F, Nussbaum C, et al. Geometry and properties of the excavation induced fractures at the Meuse/Haute-Marne URL drifts. *Rock Mech Rock Eng*. 2014;47:21–41.